AGU PUBLICATIONS

Geophysical Research Letters

RESEARCH LETTER
10.1002/2014GL060402

Key Points:
- Observational proof of resonant ocean response near the critical latitude
- Resonant responses are much stronger than the pure diurnal wind-forced currents
- Wind transfer function analysis across the latitude

Correspondence to:
S. Y. Kim,
syongkim@kaist.ac.kr

Citation:
Kim, S. Y., and G. Crawford (2014), Resonant ocean current responses driven by coastal winds near the critical latitude, *Geophys. Res. Lett.*, *41*, 5581–5587, doi:10.1002/2014GL060402.

Received 2 MAY 2014
Accepted 18 JUL 2014
Accepted article online 24 JUL 2014
Published online 13 AUG 2014

Resonant ocean current responses driven by coastal winds near the critical latitude

Sung Yong Kim[1] and Greg Crawford[2,3]

[1]Division of Ocean Systems Engineering, School of Mechanical, Aerospace and Systems Engineering, Korea Advanced Institute of Science and Technology, Daejeon, Republic of Korea, [2]Faculty of Science and Technology, Vancouver Island University, Nanaimo, British Columbia, Canada, [3]Now at the Faculty of Science, University of Ontario Institute of Technology, Oshawa, Ontario, Canada

Abstract The currents forced by wind stress near the critical latitude (30°N or 30°S) appear enhanced as a result of the combination of natural modes of ocean currents (e.g., near-inertial motions) and diurnal land/sea breeze-driven currents. Here we assess the wind-current transfer function, derived from observations of coastal surface currents and surface winds off the U.S. West Coast (32°N to 47°N), as a function of the latitude (alongshore direction) and frequency. We compare the transfer functions at the diurnal frequency derived from observations and two analytical models (e.g., the Ekman model and a near-surface averaged Ekman model). The amplitude of the data-derived transfer function decreases with increasing distance from the critical latitude, and its argument varies nearly within the range estimated from two analytical models. Our results confirm that the resonant wind-current responses near the critical latitude are 8 to 12 times stronger than the purely diurnal land/sea breeze-forced currents in other latitudes.

1. Introduction

Any moving objects on the rotating Earth are influenced by Coriolis effects and have a natural resonant frequency as a function of latitude, equal to the inertial frequency [$f_c = 2\sin\theta$ cycles per day (cpd), where θ is the latitude] [*Stewart*, 2006]. The regional currents forced by wind stress have a maximum response at the local inertial frequency as a natural resonance of ocean currents [e.g., *Ekman*, 1905; *Gonella*, 1972; *Craig*, 1989a; *Kim et al.*, 2009]. This natural resonance is based on the fact that the vertical gradient of wind stress is balanced with the Coriolis effects and the acceleration of currents [e.g., *Vallis*, 2006].

Similarly, the natural resonance appears when the energy at the inertial frequency is excited by the driving force such as broadband wind stress or impulsive wind stress imposed on the ocean at rest [e.g., *Crawford and Large*, 1996; *Elipot and Gille*, 2009]. This resonant response can be enhanced in the coastal regions near the critical latitude (30°N or 30°S) because the diurnal variability associated with land/sea breezes matches the local inertial frequency ($|f_c| = 1$ cpd) [*Haurwitz*, 1947; *Estoque*, 1961].

Thus, the wind-current response in the frequency domain shows a peak at the inertial frequency corresponding to the latitude and decreases as one moves away from that latitude. These resonant wind-current responses at the critical latitude have been addressed in a variety of theoretical studies [e.g., *Shaffer*, 1972; *Simpson et al.*, 2002; *Stockwell et al.*, 2004; *Hyder et al.*, 2002]. [*Craig*, 1989a, 1989b], in particular, derived analytical solutions for the vertical profile of horizontal currents near 30° latitude, based on a constant eddy viscosity and a periodic wind stress at a single frequency. A number of observational and numerical simulation studies of near-inertial oscillations have also been conducted [e.g., *Rosenfeld*, 1988; *Chen et al.*, 1996; *DiMarco et al.*, 2000]. However, it has been difficult to investigate those phenomena from the observations because the observed winds and currents have been insufficient to capture the latitudinal variation at the diurnal frequency [e.g., *Pidgeon and Winant*, 2005; *Edwards*, 2008; *Nam and Send*, 2013].

The input of surface wind energy through the air-sea interface is a crucial factor in upper ocean mixing, changes in the potential energy, and dissipation [e.g., *Price et al.*, 1986; *Crawford and Large*, 1996]. In particular, the resonance between air and sea interactions can play a significant role in upwelling and vertical mixing process as the resonant winds can increase the acceleration of the velocity field, which generates surface shear-driven vertical mixing [e.g., *Crawford and Large*, 1996; *Skyllingstad et al.*, 2000; *Zhang et al.*, 2009; *Orlić et al.*, 2011]. Furthermore, the diurnal wind over a stratified water column may generate diurnal inter-

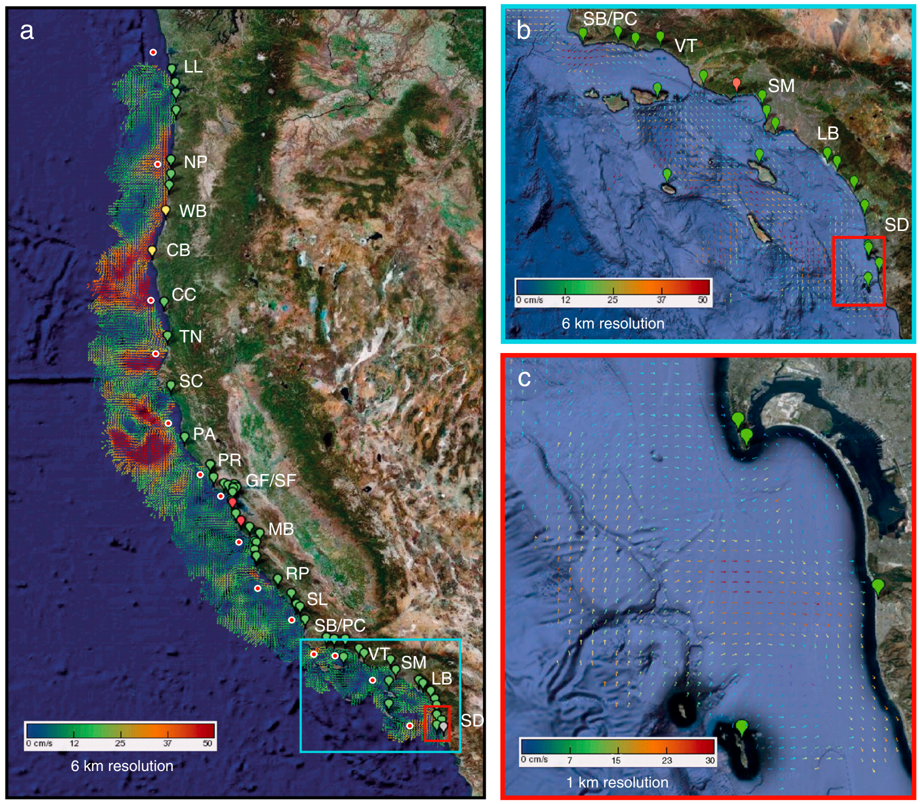

Figure 1. An example of the hourly cascade surface current maps observed by an array of high-frequency radar network on (a) the U.S. West Coast, (b) Southern California, and (c) southern San Diego. The grid resolutions of surface current maps are 6 km for Figures 1a and 1b and 1 km for Figure 1c. The HFR sites are indicated with balloons, and their latency in the near-real-time status is shown as colors (e.g., green, yellow, red, and gray). About 100 km diameter mesoscale counterclockwise eddy appears off Point Arena along with the equatorward wind event off Oregon coast (Figure 1a), and about 15 km counterclockwise diameter eddy was observed in the Santa Barbara Channel (Figure 1b). The white circles with red dots indicate the NDBC wind buoys. As a reference, major coastal regions are denoted by abbreviated two-letter names from south to north: San Diego (SD), Long Beach (LB), Santa Monica (SM), San Buenaventura (VT), Santa Barbara (SB), Point Conception (PC), Port San Luis (SL), Ragged Point (RP), Monterey Bay (MB), Gulf of the Farallones (GF), San Francisco (SF), Point Reyes (PR), Point Arena (PA), Shelter Cove (SC), Trinidad (TN), Crescent City (CC), Cape Blanco (CB), Winchester Bay (WB), Newport (NP), and Loomis Lake (LL).

nal waves [e.g., *Price et al.*, 1986; *Craig*, 1989a; *Simpson et al.*, 2002; *Hyder et al.*, 2002; *Davies*, 2003; *Davies and Xing*, 2003].

This work presents an observational proof to verify the theoretical and analytical solutions regarding the resonant response at the critical latitude and a capability of the high-frequency radar (HFR) network to inform oceanographic studies. We analyzed the HFR-derived surface currents and coastal winds at the National Data Buoy Center (NDBC) buoys off the U.S. West Coast (USWC; 32°N to 47°N) for 2 years (2008 to 2009) (Figure 1a and section 2). The data-derived wind transfer function at the diurnal frequency is compared with transfer functions estimated from two analytical models (section 3). Then, the conclusion and discussion are followed (section 4).

2. Data Analysis

2.1. Data

The HFR-derived coastal surface currents off the USWC contain mixed responses to meteorological and oceanographic forces and their interactions: locally and remotely wind-coherent components including poleward and equatorward propagating signals, barotropic and baroclinic tide-coherent currents, near-inertial motions, geostrophic currents balanced with cross-shore pressure gradients at low frequency, and currents generated by nonlinear interactions of pure tidal/inertial currents and persistent and

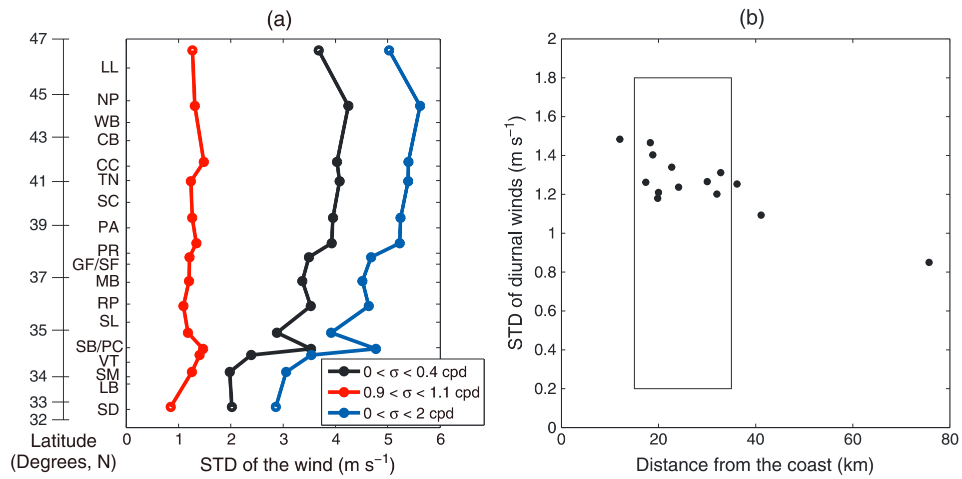

Figure 2. (a) Standard deviation (STD; square root of variance) of the wind in three frequency bands—low-frequency band ($0 < \sigma < 0.4$ cpd), diurnal band ($0.9 < \sigma < 1.1$ cpd), and broadband ($0 < \sigma < 2$ cpd)—off the USWC for 15 years (1995 to 2009). (b) STD of the diurnal wind is presented as a function of distance from the coast. A black box indicates the approximate range where HFR-derived surface currents are sampled.

intermittent eddies ranging from submesoscale to mesoscale [e.g., *Kim et al.*, 2011]. An example of cascade maps of observed surface currents off the USWC (6 km resolution; Figure 1a), Southern California (6 km resolution; Figure 1b), and southern San Diego (1 km resolution; Figure 1c) is shown. The hourly radial velocity maps obtained from 71 HFRs (as of January 2010) are optimally interpolated on the coastline-following axis, which is a spline curve grid with a 20 km resolution, located at 15 to 20 km from the shoreline [e.g., *Kim et al.*, 2011, 2013]. The radial velocity maps, sampled at the polar coordinate with a range resolution of 1.5 km to 5 km and an azimuthal resolution of 1° to 5°, are bin averaged to make them comparable in the spatial resolution (e.g., 5 km range and 5° azimuthal resolutions) before they are interpolated in order to minimize the spatial bias in the vector currents [e.g., *Kim et al.*, 2011].

The variability of hourly coastal surface winds at 14 NDBC buoys off the USWC is characterized by subinertial alongshore winds and diurnal land/sea breezes [e.g., *Dorman and Winant*, 1995; *Kim*, 2014]. The subinertial winds explain 50% to 80% of total variance, and the diurnal and its harmonically related winds account for 10% to 25% of total variance (Figure 2a). The variance of diurnal winds (within 1 ± 0.1 cpd) is nearly uniform over the entire USWC (Figure 2a) and shows a slight dependence on the distance from the shoreline due to the development of the marine boundary layer (Figure 2b) [e.g., *Estoque*, 1961; *Atkins and Wakimoto*, 1997].

2.2. Transfer Function Analysis

The transfer function analysis provides an assessment of the spectral relationship of the wind-current system within the statistical framework and has been interpreted in the dynamical framework [e.g., *Gonella*, 1972; *Kim et al.*, 2009]. From the linear parameterization between wind stress ($\hat{\boldsymbol{\tau}}$) and detided surface currents ($\hat{\mathbf{u}}$) in the frequency domain (σ),

$$\hat{\mathbf{u}}\,(\mathbf{x},\sigma) = \mathbf{H}(\mathbf{x},\sigma)\hat{\boldsymbol{\tau}}(\mathbf{x},\sigma), \tag{1}$$

the wind transfer function [$\mathbf{H}(\mathbf{x},\sigma)$] can be estimated with

$$\mathbf{H}\,(\mathbf{x},\sigma) = \frac{\langle \hat{\mathbf{u}}(\mathbf{x},\sigma)\hat{\boldsymbol{\tau}}^{\dagger}(\mathbf{x},\sigma)\rangle}{\langle \hat{\boldsymbol{\tau}}(\mathbf{x},\sigma)\hat{\boldsymbol{\tau}}^{\dagger}(\mathbf{x},\sigma)\rangle + \langle \epsilon\epsilon^{\dagger}\rangle}, \tag{2}$$

where $\langle \epsilon\epsilon^{\dagger}\rangle$ is the error covariance of the wind observations or the regularization matrix to adjust the overfitting and underfitting of the regression [*Kim et al.*, 2009] (see Appendix A for more details). The vector quantities of wind stress and surface currents can be considered as (1) a scalar combined with a complex notation for the isotropic analysis or (2) individual vector components for the anisotropic analysis. Although the anisotropic transfer function can separate the time lag and veering angle, the isotropic transfer function is more useful and convenient to present the statistical relationship between wind stress and currents

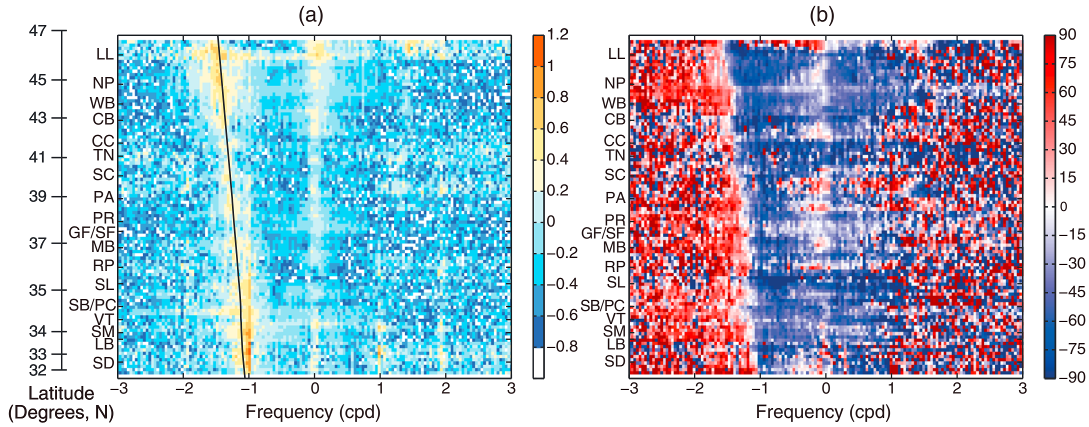

Figure 3. (a) Magnitude ($\log_{10}$ scale, $kg^{-1}\ m^2\ s$) and (b) argument (degrees) of the isotropic wind transfer function estimated from observations of HFR-derived coastal surface currents and wind stress at NDBC buoys off the USWC for 2 years (2008 to 2009), adapted from *Kim et al.* [2011]. A black line in Figure 3a indicates the local inertial frequency.

[e.g., *Kim et al.*, 2009]. In this paper, the isotropic wind transfer functions are estimated without any rotation of either winds or surface currents in order to maintain a consistent directional convention and to avoid ambiguity between the time lag and veering angle. Additionally, the transfer functions are computed from a pair of the times series of the surface current at a grid point on the coastline axis and the coastal wind at a nearby buoy. As there is no alongshore interpolation of the wind field, the estimated transfer function can be segmented or appear discontinuous (see *Kim et al.* [2013] for more details on the isotropic transfer function estimates).

Alternatively, the daily composite mean of time series can be used as a part of the time domain analysis. However, the long-term records contain seasonal modulations which result from the variation of the daily heat flux associated with the length of day. Thus, the simple composite mean of the time series without scaling the length of day can distort the phase information. Moreover, when the time series contain mixed responses due to other driving forces (e.g., wind and tides), the responses driven by other forces (e.g., tidal currents here) should be isolated in advance. As all observations in this paper are obtained from the Northern Hemisphere, the dominant rotational tendency and variability is clockwise. Thus, the diurnal frequency in this paper corresponds to −1 cpd as the clockwise motion appears in the negative frequency axis.

As the first seasonal harmonic frequency of the diurnal frequency is equal to the K_1 tidal frequency [= 1 cpd + 1/365.2425 cpd = 1.0027 cpd], we removed the barotropic diurnal tidal components at K_1, O_1, and P_1 frequencies from the surface current time series using a least squares fit prior to the wind transfer function estimate.

3. Results

The USWC-wide isotropic wind transfer function shows the enhanced amplitudes and the transition of arguments from positive ($\sigma < -f_c$) to negative ($\sigma > -f_c$) at the local inertial frequency (Figure 3). These features describe the near-inertial oscillations, driven by broadband wind stress. At higher frequencies ($|\sigma| > 3$ cpd), the fluctuation of amplitudes and arguments can be related to the noise in the observations. At low frequency ($\sigma < 0.2$ cpd), the enhanced variance in the transfer function is associated with the geostrophic currents driven by wind piled up waters against the coast (Figure 3a) [e.g., *Kim et al.*, 2009].

At the clockwise diurnal frequency ($\sigma = -1$ cpd), the magnitude of transfer functions decreases from Southern California (32.5°N) to Northern California (42°N) then slightly increases or becomes constant in the area above 42°N (Figures 3 and 4a). As the variance of diurnal land/sea breezes is nearly constant over the entire USWC (Figure 2a), the wind response can be divided into two components: a nearly uniform response due to diurnal land/sea breezes (A in Figure 4a) and an enhanced near-inertial response due to broadband wind stress (B in Figure 4a). Thus, we conclude that the broadband wind-driven near-inertial currents near the critical latitude are 8 to 12 times more than the diurnal wind-driven currents (Figure 4a),

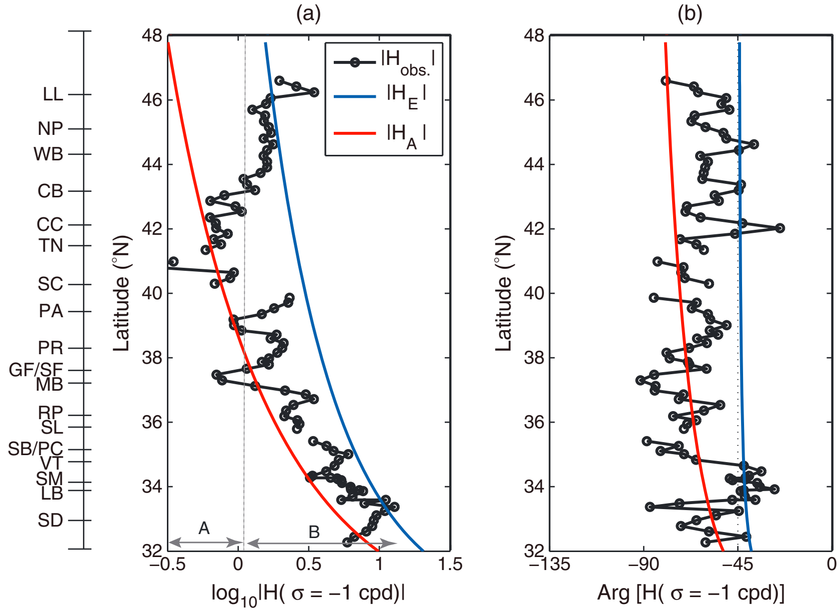

Figure 4. (a) Magnitude ($\log_{10}$ scale, kg^{-1} m^2 s) and (b) argument (degrees) of the isotropic wind transfer function at the diurnal frequency ($\sigma = -1$ cpd) estimated from observations (black), the Ekman model ($\mathbf{H}_E$; blue), and the near-surface averaged Ekman model ($\mathbf{H}_A$; at $z^* = 0.35\delta_E$, where δ_E is the Ekman depth; red) are presented in the latitude space. A gray reference line in Figure 4a divides the resonant response into the diurnal wind-driven components, which is nearly uniform over the USWC (A), and the broadband wind-driven near-inertial oscillations, which is enhanced near the critical latitude (B).

which results from the resonance at the critical latitude. The argument of the data-derived transfer function at $\sigma = -1$ cpd varies between $-45°$ and $-75°$ (Figure 4b).

The transfer functions derived from two analytical models, the Ekman model ($\mathbf{H}_E$),

$$\mathbf{H}_E(z, \sigma) = \frac{e^{\lambda z}}{\lambda \rho \nu}, \tag{3}$$

where $\lambda = \sqrt{\left[i\left(\sigma + f_c\right) + r\right] / \nu}$ [e.g., *Gonella*, 1972; *Krauss*, 1972; *Kim et al.*, 2009] (ν, ρ, and r denote the kinematic viscosity, the water density, and the frictional coefficients, respectively) and a near-surface averaged Ekman model ($\mathbf{H}_A$, $z^* = 0.35\delta_E$, δ_E is the Ekman depth),

$$\mathbf{H}_A(\sigma) = \frac{1}{z^*}\int_0^{z^*} \mathbf{H}_E(z, \sigma)\, dz, \tag{4}$$

$$= \frac{1}{z^*}\frac{1}{\lambda^2 \rho \nu}\left(e^{\lambda z^*} - 1\right), \tag{5}$$

are compared with the data-derived transfer function (Figure 4). The amplitudes of the model transfer functions are scaled by a constant ($10^{2.5}$) to compensate the difference with the data-derived transfer function, and the friction ($r = 1 \times 10^{-6}$ s^{-1}) and viscosity ($\nu = 5 \times 10^{-5}$ m^2 s^{-1}) are assumed to approximate the data-derived model and two analytical models. Moreover, the averaging depth ($z^* = 0.35\delta_E$) was chosen as the lower limit of the amplitude and phase to explain the variation of the data-derived transfer function.

The amplitudes and arguments of the data-derived transfer functions vary, for the most part, between the corresponding values of two analytical models, respectively. As the argument is a sensitive quantity, the anomalous values are excluded (representing 5% of the number of total estimates). Since HFR surface currents are taken into account as the currents averaged from the surface to $O(1)$ m depth [e.g., *Stewart and Joy*, 1974; *Barrick et al.*, 1977], the near-surface averaged Ekman model may provide the lower bound of the transfer functions. The slab layer model [e.g., *Pollard and Millard*, 1970; *D'Asaro*, 1985] was ruled out in this paper because it results in the wind-driven currents within the mixed layer which are in quadrature with wind stress at all frequencies, i.e., −90° ($\sigma < -f_c$) and 90° ($\sigma \geq -f_c$) [e.g., *D'Asaro*, 1985], which is not consistent with the HFR-derived surface current observations.

The argument averaged over the whole domain (32°N to 47°N) is approximately −60°, and there is a variation of the phase in the alongshore direction (e.g., Southern California (−45°), Northern California (−75°), and Oregon), which may be associated with the effective penetrating depth of the wind momentum in the alongshore direction.

4. Conclusion and Discussion

The resonant current response driven by wind stress near the critical latitude (30°N) is examined with the data- and model-derived transfer functions at the diurnal frequency. The transfer function analysis implements the normalization of wind forcing, which is required to compare the cross-latitudinal resonant wind-current response. The data-derived transfer function is estimated from the observed HFR-derived surface currents and winds at NDBC buoys off the USWC (32°N to 47°N). This unique alongshore-wide observation can provide a framework to investigate the alongshore variability near the coast including the resonant responses at the diurnal frequency, coastally trapped waves, and near-surface turbulence studies [e.g., *Kim et al.*, 2013; *Orton et al.*, 2010]. Our results show that the resonant wind-current responses near the critical latitude are 8 to 12 times stronger than the purely diurnal land/sea breeze-forced currents in other latitudes.

In the isotropic transfer function analysis used here, we combined the time lag and veering angle between wind stress and currents into a single term of the phase as *Pidgeon and Winant* [2005] and *Nam and Send* [2013] have done. Although this isotropic transfer function analysis may sacrifice the physical interpretation of the time lag and veering angle, it can be taken into account as a valuable geographical and statistical approach that really helps with the understanding of how much enhancement there is of diurnal wind-current interaction near and away from the critical latitude. Furthermore, the proposed analysis incorporates the normalization of wind stress to the observed currents at multiple latitudes, which can complement a study having the limited variation of local inertial frequencies [e.g., *Pidgeon and Winant*, 2005; *Edwards*, 2008; *Nam and Send*, 2013].

At the critical latitude, the near-inertial oscillations can be driven by both diurnal wind stress and diurnal tide. As the diurnal wind stress is phase locked with the heat flux variation due to sunset and sunrise, the diurnal wind stress and diurnal tide may not be coherent. However, both seasonally modulated diurnal wind stress and the K_1 tide may generate the strongly resonant near-inertial response at the critical latitude, and their interactions may attract interest.

Appendix A: An Inverse Method to Estimate the Transfer Function

The Fourier coefficients of the wind stress (**G**) and current response (**d**) are linearly parameterized with model coefficients **m**, i.e., a transfer function (see equation (1)):

$$\mathbf{d} = \mathbf{G}\mathbf{m}. \tag{A1}$$

The model coefficients are formulated with

$$\hat{\mathbf{m}} = \mathbf{P}\mathbf{G}^{\dagger}\left(\mathbf{G}\mathbf{P}\mathbf{G}^{\dagger} + \mathbf{R}\right)^{-1}\mathbf{d}, \tag{A2}$$

where **P** and **R** denote the model and error covariance matrices as the prior information of the inverse method [e.g., *Wunsch*, 1996] († denotes the matrix transpose). When they are assumed to be diagonal matrices, $\mathbf{P} = \alpha^2\mathbf{I}_\alpha$ and $\mathbf{R} = \beta^2\mathbf{I}_\beta$, respectively, where both α and β are the scalar quantities and real numbers and $\mathbf{I}_\alpha$ and $\mathbf{I}_\beta$ are the identity matrices with the different size, the transfer function can be estimated with

$$\hat{\mathbf{m}} = \mathbf{G}^{\dagger}\left(\mathbf{G}\mathbf{G}^{\dagger} + \mathbf{Q}\right)^{-1}\mathbf{d}, \tag{A3}$$

where **Q** denotes the regularization matrix representing the observational errors of wind stress and can be assumed as a diagonal matrix ($\mathbf{Q} = \gamma^2\mathbf{I}$, $\gamma^2 = \beta^2/\alpha^2$). Then, equation (A3) is equivalent to equation (2).

Acknowledgments
Sung Yong Kim is supported by the Basic Science Research Program through the National Research Foundation (NRF), Ministry of Education (2013R1A1A2057849) and the Human Resources Development of the Korea Institute of Energy Technology Evaluation and Planning (KETEP), Ministry of Trade, Industry and Energy (20134030200300), Republic of Korea. Data from this report originate from the following universities and research organizations on the USWC: Scripps Institution of Oceanography (SIO) at University of California, San Diego; University of Southern California; Marine Science Institute at University of California, Santa Barbara; California Polytechnic State University; Naval Postgraduate School, Romberg Tiburon Center at San Francisco State University; Humboldt State University; Bodega Marine Laboratory at University of California, Davis; and Oregon State University. Three USWC IOOS regional observing systems—SCCOOS, CeNCOOS, and NANOOS—are acknowledged for their continued support and advocacy of HFR current measurements for monitoring the oceans. The wind data are provided by the National Data Buoy Center (NDBC).

The Editor thanks two anonymous reviewers for their assistance in evaluating this paper.

References

Atkins, N. T., and R. M. Wakimoto (1997), Influence of the synoptic-scale flow on sea breezes observed during CaPE, *Mon. Weather Rev.*, *125*, 2112–2130.

Barrick, D. E., M. W. Evans, and B. L. Weber (1977), Ocean surface currents mapped by radar, *Science*, *198*(4313), 138–144.

Chen, C., R. Reid, and W. Nowlin Jr. (1996), Near-inertial oscillations over the Texas-Louisiana shelf, *J. Geophys. Res.*, *101*(C2), 3509–3524.

Craig, P. D. (1989a), Constant-eddy-viscosity models of vertical structure forced by periodic winds, *Cont. Shelf Res.*, *9*(4), 343–358.

Craig, P. D. (1989b), A model of diurnally forced vertical current structure near 30° latitude, *Cont. Shelf Res.*, *9*(11), 965–980.

Crawford, G. B., and W. G. Large (1996), A numerical investigation of resonant inertial response of the ocean to wind forcing, *J. Phys. Oceanogr.*, *26*(6), 873–891.

D'Asaro, E. A. (1985), The energy flux from the wind to the near-inertial motions in the surface mixed layer, *J. Phys. Oceanogr.*, *15*(8), 1043–1059.

Davies, A., and J. Xing (2003), Processes influencing wind-induced current profiles in near coastal stratified regions, *Cont. Shelf Res.*, *23*(14–15), 1379–1400.

Davies, A. M. (2003), On the interaction between internal tides and wind-induced near-inertial currents at the shelf edge, *J. Geophys. Res.*, *108*(C3), 3099, doi:10.1029/2002JC001375.

DiMarco, S. F., M. K. Howard, and R. O. Reid (2000), Seasonal variation of wind-driven diurnal current cycling on the Texas-Louisiana continental shelf, *Geophys. Res. Lett.*, *27*(7), 1017–1020, doi:10.1029/1999GL010491.

Dorman, C. E., and C. D. Winant (1995), Buoy observations of the atmosphere along the West Coast of the United States, 1981-1990, *J. Geophys. Res.*, *100*(C8), 16,029–16,044, doi:10.1029/95JC00964.

Edwards, C. R. (2008), Coastal ocean response to near-resonant sea breeze/land breeze near the critical latitude in the Georgia Bight, PhD thesis, University of North Carolina-Chapel Hill, Orlando, Fla.

Ekman, V. W. (1905), On the influence of the Earth's rotation on ocean-currents, *Ark. Mat. Astron. Fys.*, *2*, 1–53.

Elipot, S., and S. T. Gille (2009), Ekman layers in the Southern Ocean: Spectral models and observations, vertical viscosity and boundary layer depth, *Ocean Sci.*, *5*, 115–139.

Estoque, M. A. (1961), A theoretical investigation of the sea breeze, *Q. J. R. Meteorol. Soc.*, *87*, 136–140, doi:10.1002/qj.49708737203.

Gonella, J. (1972), A rotary-component method for analysis in meteorological and oceanographic vector time series, *Deep Sea Res.*, *19*, 833–846.

Haurwitz, B. (1947), Comments on the sea-breeze circulation, *J. Meteorol.*, *4*(1), 1–8.

Hyder, P., J. H. Simpson, and S. Christopoulos (2002), Sea-breeze forced diurnal surface currents in the Thermaikos Gulf, North-West Aegean, *Cont. Shelf Res.*, *22*, 585–601.

Kim, S. Y. (2014), A statistical description on the wind-coherent responses of sea surface heights off the U.S. West Coast, *Ocean Dyn.*, *64*(1), 29–46, doi:10.1007/s10236-013-0668-3.

Kim, S. Y., B. D. Cornuelle, and E. J. Terrill (2009), Anisotropic response of surface currents to the wind in a coastal region, *J. Phys. Oceanogr.*, *39*(6), 1512–1533, doi:10.1175/2009JPO4013.1.

Kim, S. Y., et al. (2011), Mapping the U.S. West Coast surface circulation: A multiyear analysis of high-frequency radar observations, *J. Geophys. Res.*, *116*, C03011, doi:10.1029/2010JC006669.

Kim, S. Y., et al. (2013), Poleward propagating subinertial alongshore surface currents off the U.S. West Coast, *J. Geophys. Res. Oceans*, *118*, 6791–6806, doi:10.1002/jgrc.20400.

Krauss, W. (1972), Wind-generated internal waves and inertial-period motions, *Dtsch. Hydrogr. Z.*, *25*(6), 241–250.

Nam, S., and U. Send (2013), Resonant diurnal oscillations and mean alongshore flows driven by sea/land breeze forcing in the coastal Southern California Bight, *J. Phys. Oceanogr.*, *43*(3), 616–630.

Orlić, M., G. Beg Paklar, V. Dadić, N. Leder, H. Mihanović, M. Pasarić, and Z. Pasarić (2011), Diurnal upwelling resonantly driven by sea breezes around an Adriatic Island, *J. Geophys. Res.*, *116*, C09025, doi:10.1029/2011JC006955.

Orton, P. M., C. J. Zappa, and W. R. McGillis (2010), Tidal and atmospheric influences on near-surface turbulence in an estuary, *J. Geophys. Res.*, *115*, C12029, doi:10.1029/2010JC006312.

Pidgeon, E. J., and C. D. Winant (2005), Diurnal variability in currents and temperature on the continental shelf between Central and Southern California, *J. Geophys. Res.*, *110*, C03024, doi:10.1029/2004JC002321.

Pollard, R. T., and R. C. Millard (1970), Comparison between observed and simulated wind-generated inertial oscillations, *Deep Sea Res.*, *17*, 813–821.

Price, J. F., R. A. Weller, and R. Pinkel (1986), Diurnal cycling: Observations and models of the upper ocean response to diurnal heating, cooling, and wind mixing, *J. Geophys. Res.*, *91*(C7), 8411–8427.

Rosenfeld, L. K. (1988), Diurnal period wind stress and current fluctuations over the continental shelf off Northern California, *J. Geophys. Res.*, *93*(C3), 2257–2276.

Shaffer, G. (1972), A theory of time-dependent upwelling induced by a spatially and temporally varying wind with emphasis on the effects of a sea breeze-land breeze cycle, *Kieler Meeresforschungen*, *28*, 139–161.

Simpson, J. H., P. Hyder, T. P. Rippeth, and I. M. Lucas (2002), Forced oscillations near the critical latitude for diurnal-inertial resonance, *J. Phys. Oceanogr.*, *32*, 177–187.

Skyllingstad, E. D., W. Smyth, and G. Crawford (2000), Resonant wind-driven mixing in the ocean boundary layer, *J. Phys. Oceanogr.*, *30*(8), 1866–1890.

Stewart, R. H. (2006), *Introduction to Physical Oceanography*, Dept. of Oceanogr., Texas A & M University.

Stewart, R. H., and J. W. Joy (1974), HF radio measurements of surface currents, *Deep Sea Res.*, *21*, 1039–1049.

Stockwell, R. G., W. G. Large, and R. F. Milliff (2004), Resonant inertial oscillations in moored buoy ocean surface winds, *Tellus*, *56A*, 536–547.

Vallis, G. K. (2006), *Atmospheric and Oceanic Fluid Dynamics*, 745 pp., Cambridge Univ. Press, Cambridge, U. K.

Wunsch, C. (1996), *The Ocean Circulation Inverse Problem*, 442 pp., Cambridge Univ. Press, New York.

Zhang, X., S. F. DiMarco, D. C. Smith, M. K. Howard, A. E. Jochens, and R. D. Hetland (2009), Near-resonant ocean response to sea breeze on a stratified continental shelf, *J. Phys. Oceanogr.*, *39*(9), 2137–2155, doi:10.1175/2009JPO4054.1.